Optical Engineering Editorial Schedule

Manuscript submissions for the following special sections should be sent to the appropriate Guest Editor listed below.

July 2005

In Memory of Academician Vladimir E. Zuev: A Legacy in Atmospheric Optics

Guest Editor:
Mikael Ciftan
U. S Army Research Office
PO Box 12211
Research Triangle Park, NC 27709
919/549-4236; 919/549-4384 FAX
E-mail: mikael.ciftan@us.army.mil

Gennady G. Matvienko
Institute of Atmospheric Optics
1, Academicheskii av.
634055, Tomsk, Russia
(3822) 259738; (3822) 259086 FAX
E-mail: magg@iao.ru

Jennifer C. Ricklin
Army Research Laboratory
2800 Powder Mill Road
Adelphi, MD 20723
301/394-2535; 301/394-0225 FAX
E-mail: jricklin@arl.army.mil

Vladimir V. Zuev
Institute of Atmospheric Optics
1, Academicheskii av.
634055, Tomsk, Russia
(3822) 258482; (3822) 258385 FAX
E-mail: vvzuev@iao.ru

This special section is dedicated to the memory of a great scientist and the founder and long-time director of the Institute of Atmospheric Optics, Academician Vladimir E. Zuev. During his lifetime Academician Zuev, working with his colleagues, made significant contributions to the foundations of atmospheric optics by using laser radiation to probe the complex atmospheric processes. These contributions in turn have enabled engineers to develop new tools that measure atmospheric conditions and enable geophysical observations. Still there remain significant gaps in our understanding of the complex dynamics of the atmosphere, which in turn requires further fundamental research. This special section is intended to gather the recent fruits of our friend's pioneering work. Topics include coherence of radiation and its degradation through scattering and absorption processes in inhomogeneous media, the problems that arise when attempting to transmit laser energy through a turbulent atmosphere, the role of aerosols, nonlinear optical and polarization effects, spectroscopy relevant to probing and inverse scattering techniques, and the investigation of the stochastic nature of turbulence including factors such as the role of wind and temperature. These research efforts impact not only the sensing of the atmosphere, but also that of aqueous media, and the Earth's surface and vegetation covers-which have now become important as well. Submissions of papers in these and related topics in atmospheric optics are invited.

August 2005

Solid State Lighting

Guest Editor:
Ian T. Ferguson
Georgia Institute of Technology
School of Electrical and Computer Engineering
Atlanta, GA 30332-0250 USA
404/385-2885; 404/385-2886 FAX
E-mail: ianf@ece.gatech.edu

John Carrano
DARPA
MicroSystems Technology Office
3701 Fairfax Dr.
Arlington, VA 22203-1700 USA
703/696-2252
E-mail: jcarrano@darpa.mil

The continued developed of high-brightness LEDs based on III-nitrides and AlInGaP has led to the possibility of revolutionary new approaches for lighting and general illumination. Efficient UV/blue solid state sources fabricated from III-nitrides can be coupled to phosphors for visible color and white light generation. Red, green, and blue LEDs can be combined to make high brightness and dynamically adjustable white sources. LED structures designed to maximize the light extraction efficiency and operate at higher powers for high lumen output are now being produced. However, many material and device challenges still remain such as improving high-power efficiencies and high-temperature performance. The implementation of LEDs, and even lasers, in general lighting applications will require new lighting paradigms that are now only being considered. The most appropriate metrics for measuring LEDs for lighting applications are still being debated. There have also been rapid advances made in the development of organic and polymeric LEDs, which are now exhibiting efficiencies similar to inorganic devices. These devices may also have utility in lighting applications and are more likely to provide broad illumination sources than the point sources produced by inorganic devices. Other approaches can be taken to producing solid state lighting sources including electrode-less sources and rare earth doping of GaN. Solid state lighting technology is rapidly advancing and very large markets are waiting for new technologies that can deliver more efficient light sources. The use of LEDs in solid state lighting is the technology of the future for lighting and general illumination. Papers will cover improvements in solid state light sources and the use of these devices in lighting applications. Areas of interest include but are not limited to solid-state light sources; light-emitting diodes (growth, fabrication, and optimization); OLEDs; UV/pumped phosphors; lighting phosphor technology (YAG, tricolor, etc.) LED fabrication improvements (light and heat extraction); packaging (light and heat extraction, phosphor down conversion); LEDs and lasers in lighting applications; illumination design for general lighting; CIE and chromaticity measurements; control systems for lighting systems; building integrationl architectictural lighting; and human factors.

Color filter array demosaicking with local color distribution linearity

Yuanjie Zheng
Shanghai Jiaotong University
Institute of Image Processing and Pattern Recognition
Shanghai, China, 200030

Stephen Lin
Microsoft Research Asia
Beijing 100080, China

Jie Yang
Shanghai Jiaotong University
Institute of Image Processing and Pattern Recognition
Shanghai, China, 200030

Abstract. We propose a novel demosaicking method based on the linearity property of a local color distribution. With the proposed technique, the color filter array can be demosaicked with less "confetti" types of errors and fringe artifacts than many current demosaicking methods. Furthermore, edge details are well preserved. © *2005 Society of Photo-Optical Instrumentation Engineers.* [DOI: 10.1117/1.1906084]

Subject terms: demosaicking; Bayer patterns; color filter arrays; local color distributions.

Paper L040921RR received Dec. 2, 2004; revised manuscript received Feb. 19, 2004; accepted for publication Feb. 25, 2004; appeared online Mar. 2, 2005; published online May 23, 2005.

1 Introduction

Due to hardware limitations, the single-chip CCD or CMOS solid state sensor array in digital cameras does not measure a complete triplet of red, green, and blue color values for each pixel in an image. Instead, it captures a sparsely sampled image of each of the color planes with a sensor whose surface is covered with a color filter array (CFA). To produce a full RGB image from these subsampled color values, CFA demosaicking is then used to reconstruct the original colors.

The Bayer array[1] shown in Fig. 1 is one of the many typical CFA patterns used in digital still cameras. A variety of methods have been proposed for demosaicking such a pattern. The simplest one is linear interpolation, which does not maintain edge information well. More advanced methods[2–4] perform CFA interpolation in a manner that preserves edge details.

A property of many local edge regions is the linearity of its color distribution in RGB space,[5] which also exists for homogeneous regions. We captialize on the linearity property of local color distributions to produce a novel demosaicking method that can result in fewer demosaicking artifacts while preserving edge details better than many current demosaicking methods.

0091-3286/2005/$22.00 © 2005 SPIE

G_{11}	R_{12}	G_{13}	R_{14}	G_{15}	R_{16}	G_{17}
B_{21}	G_{22}	B_{23}	G_{24}	B_{25}	G_{26}	B_{27}
G_{31}	R_{32}	G_{33}	R_{34}	G_{35}	R_{36}	G_{37}
B_{41}	G_{42}	B_{43}	G_{44}	B_{45}	G_{46}	B_{47}
G_{51}	R_{52}	G_{53}	R_{54}	G_{55}	R_{56}	G_{57}
B_{61}	G_{62}	B_{63}	G_{64}	B_{65}	G_{66}	B_{67}
G_{71}	R_{72}	G_{73}	R_{74}	G_{75}	R_{76}	G_{77}

Fig. 1 Sample Bayer pattern.

2 Linearity Property of Local Color Distributions

As described in Ref. 5, because of the limited spatial resolution of the image array, the image plane area of an edge pixel will generally image portions of both regions that bound the edge. For an edge pixel that lies between two regions having distinct RGB color vectors I_1' and I_2', its measured RGB color vector I_0 should be a linear combination of the bounding region colors:

$$I_0 = \alpha I_1' + (1-\alpha) I_2' \tag{1}$$

where α is a value within interval [0,1]. According to this local linearity property, I_0 should be located on the line segment between I_1' and I_2' in the 3-D RGB space. The linearity property also suggests that local changes in the three color components should be consistent with one another, expressed as

$$\frac{r_0 - r_1'}{r_2' - r_0} = \frac{g_0 - g_1'}{g_2' - g_0} = \frac{b_0 - b_1'}{b_2' - b_0} \tag{2}$$

where r_k', g_k', b_k' represent respectively the red, green, and blue values of I_k', and r_0, g_0, b_0 represent respectively the red, green, and blue values of I_0.

In this work, only three consecutive pixels on a line in the CCD array tessellation are regarded as complying with the linearity property. For example, in Fig. 1, I_{21}, I_{22}, and I_{23} should be linear with regard to 4-connectivity, and I_{11}, I_{22}, and I_{33} should be linear in the sense of 8-connectivity.

3 Linearity in Demosaicking

The linearity property shown in Eq. (2) describes expected relationships among the color components of neighboring pixels. Missing components can be determined by incorporating the linearity property into the demosaicking problem.

The green channel is first interpolated. Referring to Fig. 1, we estimate G_{34} of a red CFA pixel by first computing $\alpha_1 = |G_{35} - G_{33}|$, $\alpha_2 = |G_{44} - G_{24}|$, $\beta_1 = |B_{43} - B_{25}|$, and $\beta_2 = |B_{45} - B_{23}|$. These quantities are used to determine whether pixel I_{34} is located on a vertical, horizontal, or diagonal edge. The following estimates are then used for the missing green pixel value:

$$G_{34}=\begin{cases}(G_{33}+G_{35})/2 & \text{if } \alpha_1=MP\\ (G_{24}+G_{44})/2 & \text{if } \alpha_2=MP\\ (G_{24}+G_{33})/2 & \text{if } [(\beta_1=MP)\&(|B_{avg1}-B_{23}|<|B_{avg1}-B_{45}|)]\\ (G_{35}+G_{44})/2 & \text{if } [(\beta_1=MP)\&(|B_{avg1}-B_{45}|<|B_{avg1}-B_{23}|)]\\ (G_{24}+G_{35})/2 & \text{if } [(\beta_2=MP)\&(|B_{avg2}-B_{25}|<|B_{avg2}-B_{43}|)]\\ (G_{33}+G_{44})/2 & \text{if } [(\beta_2=MP)\&(|B_{avg2}-B_{43}|<|B_{avg2}-B_{25}|)]\end{cases} \quad (3)$$

where $MP=\min(\alpha_1,\alpha_2,\beta_1,\beta_2)$, $B_{avg1}=(B_{25}+B_{43})/2$ and $B_{avg2}=(B_{23}+B_{45})/2$. In Eq. (3), the last four cases correspond to diagonal edges. For example, a diagonal edge from the lower left to upper right is addressed in the third and fourth cases. For this kind of edge, I_{34} is first grouped to either the upper left or lower right triangle formed by the edge in the 8-neighborhood, depending on which triangle has the more similar blue value. Then G_{34} is estimated by the known green values in the selected triangle. The green channel value for a blue CFA pixel can be interpolated similarly.

After demosaicking the green color plane, the blue and red values of green CFA pixels are then estimated using the linearity property as follows, using I_{44} as an example.

$$B_{44}=\begin{cases}(B_{45}+TB*B_{43})/(1+TB) & (TB\neq -1)\&(TB\neq \text{Inf})\\ (G_{44}/G_{43})B_{43} & (TB=-1)\&(G_{43}\neq 0)\\ B_{43} & (TB=-1)\&(G_{43}=0)\\ B_{43} & TB=\text{Inf}\end{cases} \quad (4)$$

where

$$TB=\begin{cases}(G_{45}-G_{44})/(G_{44}-G_{43}) & G_{44}\neq G_{43}\\ \text{Inf} & G_{44}=G_{43}\end{cases}$$

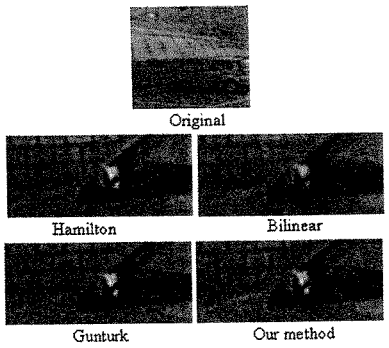

Fig. 2 Demosaicked results by some current demosaicking methods and ours on a real image.

R_{44} can be determined similarly to Eq. (4) by the known green and red components value of I_{54}, I_{44}, and I_{34}.

Linearity is also used to estimate the missing red values for blue CFA pixels, and the blue values for red CFA pixels. Using I_{54} as an example, the blue value of a red CFA pixel is interpolated as

$$B_{54}=(B_{54}^{H}+B_{54}^{V})/2 \quad (5)$$

where B_{54}^{H} is estimated from pixels I_{53}, I_{54}, and I_{55} with the method in the Eq. (4), and B_{54}^{V} is determined similarly from pixels I_{44}, I_{54}, and I_{64}.

4 Results

In our experiments, all test images are sampled with the Bayer CFA pattern and then reconstructed using demosaicking methods under comparisons in RGB color space.

In Fig. 2, we display the results of the Hamilton method,[3] the Gunturk method,[2] bilinear interpolation, and our method on a real color image. For greater clarity, we highlight a patch in the image and zoom in to obtain a larger scale. Bilinear interpolation produces many "confetti" types of artifacts. Fringe artifacts, also known as zipper artifacts, are obvious in the results of the Gunturk method. For this image, the Hamilton method performs as well as our method, both having much fewer artifacts.

More than 50 real images were tested in our experiments, and we found our method to be less susceptible to edge artifacts than these selected state-of-the-art demosaicking methods[2–4] in most cases. At the same time, our method reasonably preserves edge details. Some of the test images and demosaicking results are available on our webpage.[6]

Acknowledgments

This work was done while the first author was an intern at Microsoft Research Asia.

References

1. B. E. Bayer, "Color imaging array," U.S. Patent No. 3971065 (1976).
2. B. K. Gunturk, Y. Altunbasak, and R. M. Mersereau, "Color plane interpolation using alternating projections," *IEEE Trans. Image Process.* **11**(9), 997–1013 (2002).
3. J. F. Hamilton and J. E. Adams, "Adaptive color plane interpolation in single sensor color electronic camera," U.S. Patent No. 5629734 (1997).
4. R. Ramanath, W. E. Snyder, and G. L. Bilbro, "Demosaicking methods for Bayer color arrays," *J. Electron. Imaging* **11**(3), 306–315 (2002).
5. S. Lin, J. Gu, S. Yamazaki, and H.-Y. Shum, "Radiometric calibration from a single image," *Proc. IEEE Computer Society*, Conference on Computer Vision and Pattern Recognition, pp. 938–945 (2004).
6. www.pami.sjtu.edu.cn/people/yjzheng/research-Demosaicking.htm

Bidirectional dynamic data transmission through a rotary interface

Dagong Jia
Wencai Jing
Yimo Zhang
Guanghui Wang
Feng Tang
Jin Zhang
Tianjin University
College of Precision Instrument and Opto-electronics Engineering
Key Laboratory of Opto-electronics Information and Technical Science
Ministry of Education
Tianjing 300072, China

Abstract. A multichannel bidirectional dynamic data transmission system (DDTS) through a rotary interface with one fiber is designed based on a fabricated single pass fiber optic rotary joint. The feasibility of transmission system is tested at both 1310- and 1550-nm wavelength bands. The performance of this DDTS was measured using optical spectrum analyzer and lightwave multimeter. The insertion losses of DDTS were 1.55 and 1.20 dB at 1310- and 1550-nm wavelength bands, respectively. The total bandwidth of the DDTS is more than 170 nm. © *2005 Society of Photo-Optical Instrumentation Engineers.* [DOI: 10.1117/1.1906235]

Subject terms: dynamic data transmission; fiber optic rotary joints; wavelength division multiplexing; insertion losses; rotary interfaces.

Paper L040867 received Nov. 25, 2004; revised manuscript received Dec. 21, 2004; accepted for publication Feb. 16, 2005; appeared online Feb. 18, 2005; published online May 11, 2005.

With the rapid development of communication, a high-speed, rotating-to-fixed dynamic data transmission system (DDTS) is needed in some fields. Usually, a fiber optic rotary joint (FORJ) can be used to transmit both analog and digital signals through a rotating interface. Compared with electrical slip rings, FORJ is immune to electromagnetic interferences,[1] but has the disadvantage of high manufacturing and assembly cost.

To ensure that the optical signal is efficiently transmitted, both ends of the single-mode fiber are required to be held very closely and in proximity so that a minimal amount of light is lost in the gap.[2] In this letter, a single-channel FORJ was designed using C-lenses, the working principle and structure of which are similar to those of graded-refracted-index (GRIN) lenses.[3] Compared with GRIN lenses, the insertion loss of C-lenses is better when the working distance is longer than 50 mm.[4] Through precise mechanical design, the insertion loss of single channel FORJ is less than 2 dB at either the 1310- or 1550-nm wavelength. To enhance the capability of the FORJ, a wavelength division multiplexing (WDM) technique was adopted to increase the signal transmission capacity.[5]

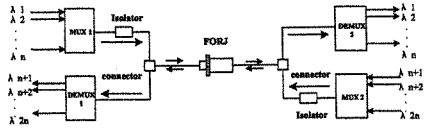

Fig. 1 Principle of dynamic data transmission system.

The working principle of DDTS is shown in Fig. 1. The wavelengths $\lambda_1, \lambda_2,\ldots,\lambda_n$ are first sent to WDM multiplexer 1 (MUX 1) where the input signals are combined into an optical single-mode (SM) fiber. Then they are sent to an isolator where the input signals are isolated from the output signals from the FORJ to reduce the noise of the dynamic transmission system. The optical signals arrive at the FORJ through the connector and are transferred across a rotating interface. Finally the received light is demultiplexed and sent into the output channels. In this way, multichannel signals from a rotary platform can be transferred to the stationary platform. At the same time, the wavelengths $\lambda_{n+1}, \lambda_{n+2},\ldots,\lambda_{2n}$ at the other end of DDTS are transmitted to MUX 2 and the input optical signals arrive at the FORJ. Then the input optical signals pass the rotating interface through the optical isolator and connector. Finally the $\lambda_{n+1}, \lambda_{n+2},\ldots,\lambda_{2n}$ are transmitted into the output channels by DEMUX 1. Because the optical components including the FORJ are all bidirectionally operable and passive components, the DDTS supports bidirectional optical transmission as well as a data transfer rate of hundreds of Gbps.

To test the feasibility of the multichannel bidirectional DDTS, an optical signal transmission system on both 1310- and 1550-nm wavelengths was designed and fabricated. A 1310/1550-nm WDM is used as the wavelength MUX and DEMUX. A 1550- and 1310-nm laser diode (LD) serve as the input light source. The 1310- and 1550-nm operating wavelengths are sent into the DEMUX/MUX in two oppo-

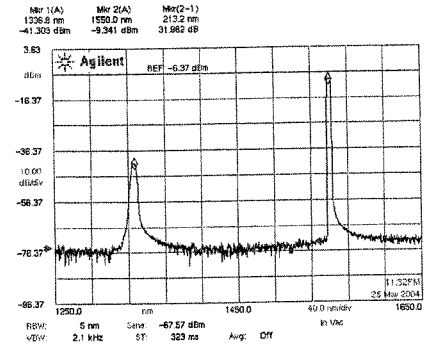

Fig. 2 Output 1 spectrum of DDTS.

0091-3286/2005/$22.00 © 2005 SPIE